2. BASIC CONCEPT AND EXPLICIT IMPLEMENTATION

Consider a finite element analysis of an earth dam (as shown in Fig. 1) or other soil structure with nonlinear, history dependent material properties, subjected to dynamic loads. The governing equations are of the form

$$\mathbf{s} + \mathbf{Cv} + \mathbf{Ma} = \mathbf{F}(t) \tag{1}$$

where, **d**, **v**, and **a** are $N_{dof} \times 1$ vectors of nodal displacements, velocities, and accelerations respectively; **M** and **C** are the mass and damping matrices respectively; **F**(t) are external nodal forces; and **s** are the internal nodal forces (discretized stress divergence). More precisely, the components of **s** represent the virtual work by the stresses due to unit virtual displacements for each of the N_{dof} degrees of freedom. Almost always, **s** is computed by numerical integration using a Gaussian quadrature formula within each element. In this case, the stresses and strains will be evaluated at a finite number, N_{int} of integration points.

Suppose there are N_ε strain components per integration point*. For the purpose of this conceptual discussion, arrange all components of strain at every integration point into one vector **E** containing a total of $N_c = N_{int}N_\varepsilon$ strain components. These strains are related to the nodal displacements **d** by an expression of the form

$$\mathbf{E} = \mathbf{Bd} \tag{2}$$

where **B** is an $N_c \times N_{dof}$ matrix that contains the strain–displacement matrices for every integration point. Unless geometrically nonlinear effects are included, **B** is constant.

Let **Σ** be a $N_c \times 1$ vector of stresses at each integration point that are conjugate to the strains **E**. The vector of internal forces (discretized stress divergence), **s**, can be written as

$$\mathbf{s} = \mathbf{B}^T\mathbf{V}\boldsymbol{\Sigma} \tag{3}$$

where **V** is a $N_c \times N_c$ diagonal matrix of tributary volumes (or areas) for each integration point.

The problem at hand is thus to solve equation 1, with the internal forces **s** being given by equation 3, and **Σ** being the stresses corresponding to strains **E** given by equation 2.

For the moment, consider integration of equation 1 using an explicit version, of the generalized integration scheme by Newmark[26], without introducing the pseudodynamic method. The procedure is as follows:

1. Start with $\mathbf{d}_n$, $\mathbf{v}_n$, and $\mathbf{a}_n$, the nodal displacements, velocities and accelerations at time $t = t_n$, as known quantities.
2. Compute the nodal velocities and displacements at time $t = t_{n+1} = t_n + \Delta t$ from
$$\mathbf{v}_{n+1} = \mathbf{v}_n + \Delta t\mathbf{a}_n \tag{4}$$
$$\mathbf{d}_{n+1} = \mathbf{d}_n + \Delta t\mathbf{v}_n + \frac{1}{2}\mathbf{a}_n\Delta t^2 \tag{5}$$

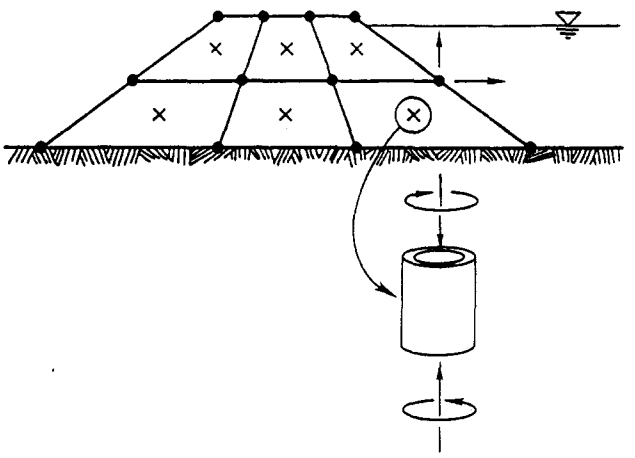

Fig. 1. Schematic representation for on-line analysis test method

3. Using a constitutive model for the soil, compute the stresses **Σ**.
4. Compute the internal forces, $\mathbf{s} = \mathbf{s}_{n+1}$, from equation 3.
5. Evaluate the nodal accelerations using equation 1:
$$\mathbf{a}_{n+1} = \mathbf{M}^{-1}(\mathbf{F}_{n+1} - \mathbf{s}_{n+1} - \mathbf{Cv}_{n+1}) \tag{6}$$
6. Increment n and repeat steps 2–5 for the next time step.

For the on−line analysis−test, the procedure is identical, except that instead of using a mathematical constitutive law in step 3, a soil sample is used for every integration point. The strains **E** are imposed on these soil samples, and the corresponding stresses **Σ** can then be measured. Thus the stress–strain relation used is that of an actual soil sample—not that of a mathematical material.

The main advantages of this method are:

a) It does not rely on idealized constitutive models for the material.
b) In a two–phase formulation of the problem discussed in Section 4, it is possible to account mathematically for pore pressure dissipation effects. This makes it possible to simultaneously model inertial and pore pressure dissipation effects.
c) Stresses, strains, pore pressure and visual inspection are available for every integration point.
d) The formation sequence of an earth structure can be faithfully followed. This is also possible for finite element modeling techniques, but a lot more difficult in centrifuge testing, for which the specimen would have to be formed in flight.
f) Any part of the structure can be modeled analytically, by replacing some of the soil samples with mathematical constitutive laws. Thus regions in which the soil behavior is well understood can be modeled analytically, while soil samples are used in other regions. It is also possible to introduce radiating boundary conditions.

As might be expected there are also a number of difficulties associated with the method:

* For one–dimensional problems, $N_\varepsilon = 1, 2$, or 3, $N_\varepsilon = 3$ for plane strain; abd $N_\varepsilon = 6$ for fully three–dimensional problems

a) Typically, in a finite element analysis, a large number of integration points are required. This means that the number of test specimens may well become impractical. A problem for which the number of integration points remains manageable is that of vertically propagating seismic waves in layered soils. Although simple, this problem is quite important in the evaluation of liquefaction potential on level ground[37]. For more complicated problems, such as the seismic response of an earth dam, the number of degrees of freedom and integration points can be reduced by use of a small number of deformation modes (Ritz vectors in a Rayleigh–Ritz approach). Such deformation modes would be based on a prior analysis of the structure with a mathematical constitutive law. For example, the deformation modes could correspond to the first few natural modes of vibration plus perhaps one or two shakedown modes to model the effect of densification produced by cyclic shear strains. The locations and tributary areas or volumes for each integration point could be calibrated in such a way that the reduced system leads to accurate solutions.

b) A test setup in which all six components of strain on a sample can be controlled independently has yet to be devised. True triaxial tests for which three principal strains can be controlled independently have been used with success[27–31]. However, these do not allow for any rotation of the principal axes*. Also accurate control of the strains is difficult in some of the true triaxial test setups. For the plane strain case, the hollow cylinder test can be used: the axial and shear strain can be controlled by axial and torsional motion of the shaft, whereas hoop and radial strains can be controlled by means of different pressures inside and outside the cylinder. Finally, a number of strategies can be used to replace complex strain paths by simpler ones. An example of this is given by Wang *et al.*[23]. The price paid for using such 'equivalent' strain paths is that the equivalence is not verified by the experiment. Thus the constitutive model is only partly experimental in this case.

c) The on–line analysis test method described above is based on explicit time integration. Shing and Mahin[32,33] have shown that this approach can lead to high sensitivity of the results to experimental errors. This is especially true for multi degree of freedom systems, which appear to experience spurious excitation of the higher modes. However, for the recently developed an implicit implementation for the pseudodynamic method applied to building structures[34], error analyses indicate that the effect of random errors is minimal, even for systems with a large number of degrees of freedom[25]. Indeed, these error analyses showed a decrease in the cumulative errors as the number of degrees of freedom was increased. In contrast to building structures, use of the implicit approach for the on–line analysis–test method requires an actuator control strategy to enforce compatibility as well as equilibrium conditions.

d) Finally, the on–line analysis–test typically would proceed slower than real time. This means that strain rate dependent material behavior may not be modeled accurately. To some extent this can be compensated for by suitable choice of a damping matrix **C**.

On balance there is little doubt that the pseudodynamic methods applied to earth structures presents some technical difficulties that are not encountered in pseudodynamic testing of buildings. However this is also true for shake table tests: Having to perform the shake table test inflight on a centrifuge certainly also increases the level of technical difficulty of such a test. For a more demanding modeling task, it is not surprising that some additional difficulties be encountered in applying the pseudodynamic concept to soil structures. The author feels that whereas some of the requirements for experimental accuracy and control tend to exceed the capabilities of current soil testing devices, the required performance levels are achievable.

3. IMPLICIT IMPLEMENTATION OF THE ON–LINE ANALYSIS–TEST METHOD

It is well known that the explicit time integration scheme described above is only conditionally stable. Indeed very small timesteps may be required to ensure stability. Furthermore, experience from implementation of the pseudodynamic test method for building structures based on explicit time integration[32,33] indicates that error propagation characteristics of the method deteriorate as the number of degrees of freedom increases. This has resulted in spurious excitation of the higher modes. An appropriate implicit time integration scheme on the other hand is unconditionally stable and has better error propagation characteristics[24]. Despite the advantages of implicit time integration, its implementation in on on–line analysis–test procedure poses some special problems, which are addressed in this section.

Following the generalized implicit time integration method by Newmark[26], the accelerations, velocities and displacements at time $t = t_{n+1} = t_n + \Delta t$ are given by:

$$\mathbf{a}_{n+1} = \frac{\mathbf{1}}{\beta(\Delta t)^2}\,\Delta\mathbf{d} \tag{7}$$

$$\mathbf{v}_{n+1} = \tilde{\mathbf{v}}_{n+1} + \frac{\gamma}{\beta\Delta t}\,\Delta\mathbf{d} \tag{8}$$

$$\mathbf{d}_{n+1} = \tilde{\mathbf{d}}_{n+1} + \Delta\mathbf{d} \tag{9}$$

where

$$\tilde{\mathbf{v}}_{n+1} = \mathbf{v}_n + (1-\gamma)\Delta t\mathbf{a}_n \tag{10}$$

$$\tilde{\mathbf{d}}_{n+1} = \mathbf{d}_n + \Delta t\mathbf{v}_n + \left(\frac{1}{2} - \beta\right)(\Delta t)^2\mathbf{a}_n \tag{11}$$

are the predictor values of the velocities and displacements,

* Except by multiples of 90° after traversing other principal strain states.

and $\Delta\mathbf{d}$ is a displacement correction which must satisfy

$$\mathbf{s}_{n+1} + \left(\frac{\gamma}{\beta\Delta t}\mathbf{C} + \frac{1}{\beta(\Delta t)^2}\mathbf{M}\right)\Delta\mathbf{d} = \tilde{\mathbf{F}}_{n+1} \tag{12}$$

where

$$\tilde{\mathbf{F}}_{n+1} = \mathbf{F}_{n+1} - \mathbf{C}\tilde{\mathbf{v}}_{n+1} \tag{13}$$

Equation (9) can be rewritten in the form:

$$\mathbf{d}_{n+1} + \tilde{\mathbf{M}}^{-1}\mathbf{s}_{n+1} = \tilde{\mathbf{d}}_{n+1} \tag{14}$$

where

$$\tilde{\mathbf{M}} = \frac{1}{\beta(\Delta t)^2}\mathbf{M} + \frac{\gamma}{\beta\Delta t}\mathbf{C} \tag{15}$$

$$\tilde{\mathbf{d}}_{n+1} = \tilde{\mathbf{d}}_{n+1} + \tilde{\mathbf{M}}^{-1}\tilde{\mathbf{F}}_{n+1} \tag{16}$$

The components of $\tilde{\mathbf{d}}_{n+1}$ will be referred to as the adjusted predictor displacements. They are fully determined from the solution for time $t = t_n$, and can therefore be regarded as known quantities in as far as finding the solution for time $t = t_{n+1}$ is concerned.

Premultiplying equation (14) by $\mathbf{B}$, and substituting for s_{n+1} from equation (3) leads to

$$\mathbf{E}_{n+1} + \mathbf{B}\tilde{\mathbf{M}}^{-1}\mathbf{B}^T\mathbf{V}\boldsymbol{\Sigma}_{n+1} = \tilde{\mathbf{E}}_{n+1} \tag{17}$$

where

$$\mathbf{E}_{n+1} = \mathbf{B}\mathbf{d}_{n+1} \tag{18}$$

are the (measurable) strains in the specimen, and

$$\tilde{\mathbf{E}}_{n+1} = \mathbf{B}\tilde{\mathbf{d}}_{n+1} \tag{19}$$

will be referred to as the adjusted predictor strains.

Once the test result for time $t = t_n$ is available, all quantities in equation (17) are known, except $\mathbf{E}_{n+1}$ and $\boldsymbol{\Sigma}_{n+1}$. The solution for time $t = t_{n+1}$ is then obtained by enforcing equation (17) together with the experimental stress–strain relationship,

$$\boldsymbol{\Sigma}_{n+1} = \boldsymbol{\Sigma}_{n+1}(\mathbf{E}_{n+1}) \tag{20}$$

Numerically, equations (17) and (20) would normally be solved by an iterative scheme requiring multiple evaluations of $\boldsymbol{\Sigma}_{n+1}(\mathbf{E}_{n+1})$. For a mathematical material, such multiple evaluations do not pose a problems, since at each iteration, the state parameters for the material would be set back to the values at the previous load step before evaluating $\boldsymbol{\Sigma}_{n+1}(\mathbf{E}_{n+1})$. However, if the stress strain relation is being determined experimentally as in an on−line analysis, multiple evaluations of $\boldsymbol{\Sigma}_{n+1}\mathbf{E}_{n+1})$ would result in a loading history for the sample that is different from that indicated by the problem. For inelastic materials, this leads to erroneous results. This difficulty also arises in pseudodynamic testing of buildings. As a result, the implicit approach was largely abandoned until recent work by Thewalt and Mahin[24]. Their method employs an experimental control strategy using force as well as displacement feedback by which equation (14) is enforced automatically without the need for any iterative computations.

The approach of Thewalt and Mahin can also be adapted to on–line analyses of earth structures. In this case, force and displacement feedback are replaced by stress and strain feedback respectively. The control circuitry for such an on−line analysis is shown in Fig. 2. Therein the soil samples box represents not only the soil samples, but also the actuators capable of producing deformations of these soil samples. The thick lines represents electrical signals that flow continually (i.e. signals that are needed at all times for control of the test), whereas the thin lines transmit reading only once at every timestep of the numerical integration scheme. The signals could be analog (voltages) with the appropriate A/D and D/A conversions, or digital. Enforcement of equation (17) is achieved by the inner control loop: The computational box generates a command signal denoted ${}^6\tilde{\mathbf{E}}$, which represents the right hand side of equation (17). The feedback consists of a linear combination of the measured strains ${}^1\mathbf{E}$ and stress ${}^1\boldsymbol{\Sigma}$ denoted ${}^1\tilde{\mathbf{E}}$. It represents the left hand side of equation (17). Any imbalance between the command signal ${}^6\tilde{\mathbf{E}}$ and the feedback ${}^1\tilde{\mathbf{E}}$ is transmitted to one or more controllers. These controllers then produce actuator motion that corrects this imbalance. As a result equation (17) is satisfied once actuator motion ceases.

In order to make the strain path from one loadstep to the next as straight as possible, the command signal is not changed suddenly. Instead it should follow some specified ramp function with a rise time that is long compared to typical actuator response times.

Studies of the stability of this inner control loop[35,36] indicate that the system is stable under a wide range of conditions. This means that the system will not overshoot the solution to equation (17) at each timestep. Furthermore, the stress feedback needed in order to implement the *implicit* Newmark scheme has a stabilizing effect on the inner control loop.

Once the solution to equation (17) has been obtained, the displacements can be computed as the solution of equation (2). This solution only exists if the strains satisfy compatibility. In general, due to control errors, the strains will not satisfy compatibility exactly. In this case, the optimum value of the displacements in the sense that the sum of the squares of the residuals are minimized is obtained as the solution of

$$(\mathbf{B}^T\mathbf{B})\mathbf{d}_{n+1} = \mathbf{B}^T\mathbf{E}_{n+1} \tag{21}$$

If there are no zero energy deformation modes, then $\mathbf{B}$ is nonsingular in the sense that

$$\mathbf{B}\mathbf{d} = \mathbf{0} \quad \text{if and only if} \quad \mathbf{d} = \mathbf{0} \tag{22}$$

This ensures that equation (17) is a sufficient as well as necessary condition for enforcing equation (14) Furthermore, the second and third terms in equation (17) represent compatible strains. Therefore the strains $\mathbf{E}_{n+1}$ which satisfy equation (17) must also be compatible. Thus equation (17) enforces compatibility as well as equilibrium. Finally, if $\mathbf{B}$ is nonsingular, $(\mathbf{B}^T\mathbf{B})$ must be positive definite and symmetric. This ensures that the solution of equation (21) can readily be computed.

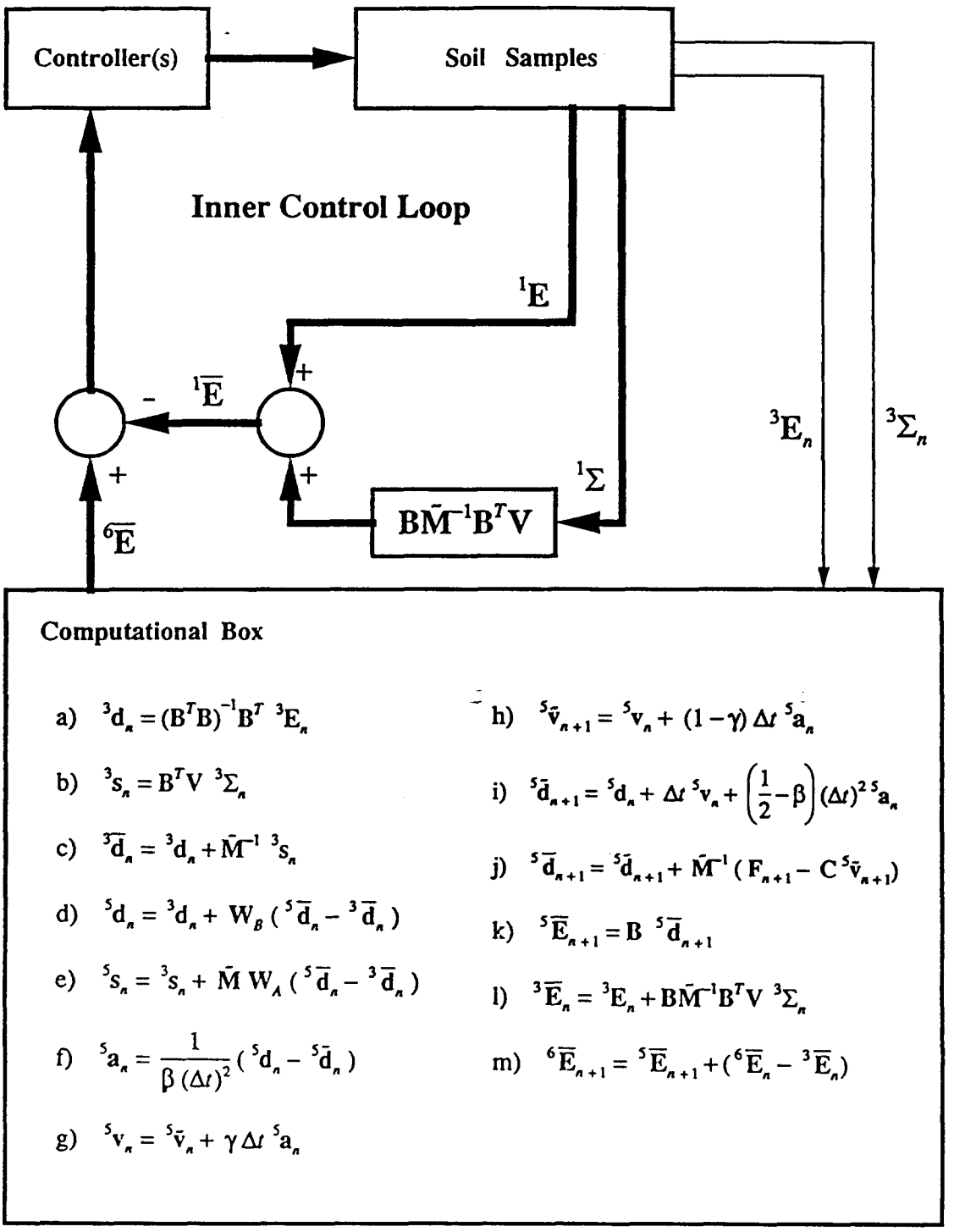

Fig. 2. Flow diagram for the implementation of the on-line analysis test method based on an implicit time integration scheme

In order for **B** to be nonsingular its number of rows must be greater or equal to its number of columns, which means that the redundancy, defined as

$$N_r = N_c - N_{dof} \tag{23}$$

must be nonnegative. Note that equation (17) represents N_c equations, which are based on N_{dof} dynamic equilibrium equations (1). The additional N_r equations arise because of the need to enforce compatibility as well as equilibrium.

4. DETAILS OF IMPLICIT IMPLEMENTATION

It is well known from control theory that it is in general impossible to enforce a control objective (such as satisfying equation (17)) exactly. There is a tradeoff between accuracy and stability of the control strategy, Since stability is essential, there will always be some control error. This control error can be monitored, but not eliminated. This section focuses on how such control errors are treated. It has been found [25] that error propagation characteristics can be quite sensitive to such details of the implementation.

The quantity that needs to be controlled in an on–line test based on implicit time integration is a linear combination of stresses and strains denoted $\bar{\mathbf{E}}$. The measured value of this quantity to be used for control purposes is denoted ${}^{1}\bar{\mathbf{E}}$ in Fig. 2. Due to tracking errors this measured adjusted predictor displacement will not be exactly equal to the command signal ${}^{6}\bar{\mathbf{E}}$. Indeed, upper left indices are used to distinguish between different values of any quantity. Specifically, the upper left indices 1 and 3 identify measured values used in control and in the computational box (Fig. 2) respectively; the left index 6 is used for the command signal; and finally it was found convenient[25] to define consistent values (upper left index 5) such that they satisfy the time–discretized equation of motion exactly. In absence of experimental errors all values of any given quantity (different upper left indices) would be equal.

During a typical cycle, the measured strains and stresses (denoted ${}^{3}\mathbf{E}_n$ and ${}^{3}\boldsymbol{\Sigma}_n$ respectively) are used in the computational box is to calculate the command signal for the next timestep ${}^{6}\bar{\mathbf{E}}_{n+1}$. This is done by evaluating the quantities shown therein in the order indicated. The command signal ${}^{6}\bar{\mathbf{E}}$ is then incremented from the value ${}^{6}\bar{\mathbf{E}}_n$ to the new value ${}^{6}\bar{\mathbf{E}}_{n+1}$, following some specified ramp function. The command signal is held at ${}^{6}\bar{\mathbf{E}}_{n+1}$ until actuator motion ceases*. By virtue of the inner loop control system, this means that the stresses and strains in the samples are the solution for timestep $t = t_{n+1}$. The procedure can then be repeated for the next timestep.

Attention is now focused on the steps in the computational box of Fig. 2: Due to control errors, the 'measured' values of displacements and resisting forces (upper left index 3), computed in Steps (1) and (b) of the computational box do not satisfy equation (14) exactly. Therefore they cannot be used as consistent values in the sense described above. Instead, one of the following possibilities is used to define consistent values:

A) Use the 'measured' value of the displacements and adjust the resisting forces to satisfy equation (14).
B) Use the 'measured' values of the resisting forces and adjust the displacements to satisfy equation (14).
C) Use a weighted average of possibilities A and B.

This last possibility is adopted here. The weighting matrices for possibilities A and B are denoted $\mathbf{W}_A$ and $\mathbf{W}_B$ respectively, and must satisfy the condition

$$\mathbf{W}_A + \mathbf{W}_B = \mathbf{I} \tag{24}$$

where $\mathbf{I}$ is the identity matrix. For $\mathbf{W}_A = \mathbf{I}$ and $\mathbf{W}_B = \mathbf{O}$, possibility A is recovered, whereas possibility B can be recovered using $\mathbf{W}_A = \mathbf{O}$ and $\mathbf{W}_B = \mathbf{I}$. Generally, error analyses[25] reveal that possibility B is preferable to possibility A. Under certain circumstances judicious choice of the weighting matrices can lead to further improvement in error propagation characteristics.

The consistent values of displacements and resisting forces are calculated in steps (c) to (e). Subsequent steps (f–k) are based directly on equations (7)–(11), (16), and (19). The adjusted predictor strains computed in step (k) represent the desired value for the left hand side of equation (17). These could be used directly as a command signal. However it is desirable to compensate for an anticipated tracking error**. This is done in steps (l) and (m). Therein the anticipated tracking error for timestep $n+1$ is taken to be the tracking error at the previous timestep n.

One of the more complicated aspects of the implementation of the stress feedback for the inner loop control is the multiplication operation in which the stress feedback ${}^{1}\boldsymbol{\Sigma}$ is multiplied by the matrix $\mathbf{B}\tilde{\mathbf{M}}^{-1}\mathbf{B}^T\mathbf{V}$. This matrix is generally fully populated. In an analog implementation of the inner control loop, this could require quite complicated circuitry. Alternatively for digital implementation, the refresh period for this digital control system needs to be small compared to typical response times of the loading mechanism. This could be achieved by a specialized external processor. The advantage of digital control is that it is generally more accurate, and also easier to change control parameters such as the elements of the matrix $\mathbf{B}\tilde{\mathbf{M}}^{-1}\mathbf{B}^T\mathbf{V}$.

5. TWO–PHASE FORMULATION

Liquefaction can be one of the most devastating effects of seismic ground motion. Therefore realistic evaluations of the liquefaction potential are essential. In most cases liquefaction is caused by the tendency for soil to densify when subjected to cyclic loading. Often undrained conditions are assumed. In this case, a single phase formulation can be used. However, in more permeable materials, such as sands, a significant portion of the pore pressures generated by soil densification are dissipated during the period of seismic excitation. In addition, pore water flow tends to attenuate the propagation of seismic waves in the medium. To account for these effects the two–phase nature of the medium must be considered.

The finite element formulation for the soil and pore fluid as a coupled system is summarized in Appendix A. For small deformations, and incompressible soil grains, the semi–discrete equations for the system are:

$$\begin{pmatrix} \mathbf{s}' \\ \cdot \end{pmatrix} + \begin{pmatrix} \mathbf{K}_s & \mathbf{K}_f \\ \mathbf{K}_f & \mathbf{K}_f \end{pmatrix}\begin{pmatrix} \mathbf{d}_s \\ \mathbf{d}_f \end{pmatrix} + \begin{pmatrix} \cdot & \cdot \\ \cdot & \mathbf{C} \end{pmatrix}\begin{pmatrix} \mathbf{v}_s \\ \mathbf{v}_f \end{pmatrix} + \begin{pmatrix} \mathbf{M} & \mathbf{M}_f \\ \mathbf{M}_f & \mathbf{M}_{ff} \end{pmatrix}\begin{pmatrix} \mathbf{a}_s \\ \mathbf{a}_f \end{pmatrix} = \begin{pmatrix} \mathbf{f} \\ \mathbf{f}_f \end{pmatrix} \tag{25}$$

in which $\mathbf{d}_s$, $\mathbf{v}_s$ and $\mathbf{a}_s$ are vectors of nodal displacements, velocities and accelerations for the soil skeleton; $\mathbf{d}_f$, $\mathbf{v}_f$ and $\mathbf{a}_f$ are vectors of nodal seepage displacements, velocities and acceleration[5]; and $\mathbf{f}$, $\mathbf{f}_f$ are equivalent nodal forces due to body forces and tractions on the solid and fluid phases, given in equations (A9) and (A10). The elements of $\mathbf{s}'$ represent the internal nodal forces

* This intermittent loading approach often used on pseudodynamic testing of building structures. Continuous testing procedures are advantageous from the point of view preventing stress relaxation effects, but place heavier demands to the control system.

**Here the term tracking error refers to the difference between the command signal ${}^{6}\mathbf{E}_m$ and the measured adjusted predictor strains ${}^{3}\mathbf{E}_n$ defined in step (l) of the computational box in Fig. 2.

[5]The seepage displacement vector is defined in Appendix A such that for any surface that moves with the soil skeleton, the dot product of the seepage displacement vector with the unit normal to that surface represents the volume of flow per unit area through that surface.

(discretized stress divergence) due to the effective stresses, given by

$$\mathbf{s}' = \mathbf{B}^T \mathbf{V} \boldsymbol{\Sigma}' \tag{26}$$

in which $\boldsymbol{\Sigma}'$ is a $N_c \times 1$ vector that contains the effective stresses in each soil sample.

Formulae for computing $\mathbf{M}$, $\mathbf{M}_f$, $\mathbf{K}_f$, and $\mathbf{C}$ are given in Appendix A. For the purpose of this discussion it suffices to note that for small deformations these are constant, symmetric matrices which can be computed before beginning the on-line test.

The first submatrix equation in equation (25) enforces overall equilibrium of the system, whereas the second ensures equilibrium of the fluid phase.

No viscous damping terms have been included in equation (25) other than that which arises due to viscosity of the pore fluid as it flows through the soil. Additional viscous damping terms could be added, if desired.

Equation (25) applies for the case that the same interpolation functions are used for seepage displacements as for the displacements of the soil skeleton. Furthermore, these equations would be modified in order to introduce displacement, or flow boundary conditions (prescribed values for some of the nodal displacements). However, such modifications, or the use of different interpolation functions for the seepage displacements and displacements of the soil skeleton does not alter the symmetry and coupling structure of equation (25).

Time discretization of equation (25) by Newmark's method is achieved by applying equations (7)–(9) to the solid and fluid phases. In order to simplify the notation the subscript $n+1$ which identifies the subscripted entity as being evaluated at time $t = t_{n+1}$ is omitted. Instead, the subscripts s and f indicate whether the entity pertains to the soil skeleton or the fluid. This leads to the following expressions for the displacements, velocities and accelerations for the soil skeleton, and those for seepage at time $t = t_{n+1}$:

$$\mathbf{a}_s = \frac{1}{\beta(\Delta t)^2}\Delta \mathbf{d}_s, \quad \mathbf{a}_f = \frac{1}{\beta(\Delta t)^2}\Delta \mathbf{d}_f \tag{27}$$

$$\mathbf{v}_s = \tilde{\mathbf{v}}_s + \frac{\gamma}{\beta \Delta t}\Delta \mathbf{d}_s, \quad \mathbf{v}_f = \tilde{\mathbf{v}}_f + \frac{\gamma}{\beta \Delta t}\Delta \mathbf{d}_f \tag{28}$$

$$\mathbf{d}_s = \tilde{\mathbf{d}}_s + \Delta \mathbf{d}_s, \quad \mathbf{d}_f = \tilde{\mathbf{d}}_f + \Delta \mathbf{d}_f \tag{29}$$

in which the predictor values (those with tildes) can be computed by applying equations (10) and (11) to the fluid and solid phases.

Substituting equations (27) to (29) into equation (25) yields,

$$\begin{pmatrix} \mathbf{s}' \\ \cdot \end{pmatrix} + \begin{pmatrix} \mathbf{K}^*_{ss} & \mathbf{K}^*_{sf} \\ \mathbf{K}^*_{fs} & \mathbf{K}^*_{ff} \end{pmatrix} \begin{pmatrix} \Delta \mathbf{d}_s \\ \Delta \mathbf{d}_f \end{pmatrix} = \begin{pmatrix} \tilde{\mathbf{f}} \\ \tilde{\mathbf{f}}_f \end{pmatrix} \tag{30}$$

in which

$$\mathbf{K}^*_{ss} = \mathbf{K}_f + \frac{1}{\beta(\Delta t)^2}\mathbf{M} \tag{31}$$

$$\mathbf{K}^*_{sf} = \mathbf{K}^*_{fs} = \mathbf{K}_f + \frac{1}{\beta(\Delta t)^2}\mathbf{M}_f \tag{32}$$

$$\mathbf{K}^*_{ff} = \mathbf{K}_f + \frac{\gamma}{\beta \Delta t}\mathbf{C} + \frac{1}{\beta(\Delta t)^2}\mathbf{M}_{ff} \tag{33}$$

$$\tilde{\mathbf{f}} = \mathbf{f} - \mathbf{K}_f(\tilde{\mathbf{d}}_s + \tilde{\mathbf{d}}_f) \tag{34}$$

$$\tilde{\mathbf{f}}_f = \mathbf{f}_f - \mathbf{K}_f(\tilde{\mathbf{d}}_s + \tilde{\mathbf{d}}_f) - \mathbf{C}\tilde{\mathbf{v}}_f \tag{35}$$

Eliminating $\Delta \mathbf{d}_f$ from equations (30) by static condensation gives

$$\mathbf{s}' + \hat{\mathbf{K}}\Delta \mathbf{d}_s = \hat{\mathbf{f}} \tag{36}$$

in which

$$\hat{\mathbf{K}} = \mathbf{K}^*_{ss} - \mathbf{K}^*_{sf}\mathbf{K}^{*-1}_{ff}\mathbf{K}^*_{fs} \tag{37}$$

$$\hat{\mathbf{f}} = \tilde{\mathbf{f}} - \mathbf{K}^*_{sf}\mathbf{K}^{*-1}_{ff}\tilde{\mathbf{f}}_f \tag{38}$$

To obtain a form that is suitable for implementation of the on-line analysis test method, substitute $\Delta \mathbf{d}_s = \mathbf{d}_s - \tilde{\mathbf{d}}_s$, and $\mathbf{s}' = \mathbf{B}^T\mathbf{V}\boldsymbol{\Sigma}'$ into equation (36), and premultiply by $\mathbf{B}\hat{\mathbf{K}}^{-1}$ to get

$$\mathbf{E} - \tilde{\mathbf{E}} + \mathbf{B}\hat{\mathbf{K}}^{-1}\mathbf{B}^T\mathbf{V}\boldsymbol{\Sigma}' = \mathbf{0} \tag{39}$$

where $\mathbf{E}$ and $\boldsymbol{\Sigma}'$ are the vectors which contain the strains and effective stresses at each soil sample (integration point in the finite element mesh), and

$$\tilde{\mathbf{E}} = \mathbf{B}\tilde{\mathbf{d}}_s \tag{40}$$

$$\tilde{\mathbf{d}}_s = \tilde{\mathbf{d}}_s + \hat{\mathbf{K}}^{-1}\tilde{\mathbf{f}} \tag{41}$$

In comparing equation (39) with equation (17), it is seen that they are in exactly the same form, the only difference being that $\tilde{\mathbf{M}}$ is replaced be a different constant matrix $\hat{\mathbf{K}}$, and the stresses $\boldsymbol{\Sigma}$ are replaced by the effective stresses $\boldsymbol{\Sigma}'$. Therefore implementation of the on-line analysis–test procedure follows in exactly the same way as before: strains in the sample are imposed under drained conditions, and the measured effective stresses are used as feedback in the analysis.

It might appear that the need to carry out the testing under drained conditions would place a severe limitation on testing speed. This turns out not to be the case, since the drainage path for the test specimen is typically much smaller than that for the prototype earth structure. Therefore even for a real-time test the effects of pore pressure gradients within the sample can be expected to be small. For a test that proceeds slower than real time, the differences on pore pressure within the specimen are even smaller.

As mentioned, the limitations in the number of soil samples that van be tested simultaneously requires a reduction is the number of degrees of freedom. However, for a given motion of the soil skeleton, seepage effects can be computed to any desired accuracy. Hence the restriction on the number of degrees of freedom applies to the soil skeleton only. Following the Rayleigh–Ritz method, the nodal displacements for the soil skeleton are expressed as

$$\mathbf{d}_s = \boldsymbol{\Phi}\mathbf{y} \tag{42}$$

in which the vector $\mathbf{y}$ contains a reduced set of generalized displacements, and $\boldsymbol{\Phi}$ is a matrix whose columns are

assumed deformation modes for the soil skeleton. It can verified that equation (39) is still applicable in this case, if **B** is replaced by $\mathbf{B}\Phi$.

6. NON-DYNAMIC PROBLEMS

In some cases it may be desirable to apply this on-line analysis-test method to a problem in which inertia effects are negligible. For example, the construction process of an earth dam, rapid drawdown conditions, or the changes in pore pressure that occur after an earthquake could be simulated. Although the formulation given here is dynamic, such static conditions can also be handeled by treating the static problem as a dynamic one. Since such non-dynamic problems typically extend over longer periods of time, it is convenient to increase the size of the timestep Δt. This can lead to problems. For the explicit implementation, the timestep must remain below the stability limit. For the implicit case, there is no stability limit (provided the parameters γ and β are suitably chosen), but the test becomes more and more force (or stress) controlled as Δt is increased. Ultimately as $\Delta t \to \infty$ the test becomes entirely force controlled. This means the enforcement of compatibility is lost in the limiting process.

One way to overcome the problems associated with larger timesteps is to artificially increase the inertial and/or damping effects. For example, the actual mass matrix of the structure could be scaled by a factor, F, larger than unity. As a result, the natural periods of the structure all increase by a factor $\sqrt{F}$. As long as the fundamental period of the structure remains very small compared to the time over the loads are applied, the artificial increase in the inertia of the structure will have negligible effect on the results. This method of using artificial mass and damping matrices is an accepted technique for solving static problems using an explicit time integration scheme.

For the implicit scheme, it is also possible to increase the timestep without loosing enforcement of the compatibility condition by amplifying the incompatible component of the feedback signal in the inner control loop. For this purpose, any vector of strains **E** can be decomposed into a compatible portion, here denoted $\mathbf{E}_{comp}$, and an incompatible portion, $\mathbf{E}_{inc}$. To make this decomposition unique it is required that the Euclidean norm of $\mathbf{E}_{inc}$ be minimized. This leads to

$$\mathbf{E}_{inc} = \mathbf{I}_{inc}\mathbf{E}, \text{ where } \mathbf{I}_{inc} = \mathbf{I} - \mathbf{B}(\mathbf{B}^T\mathbf{B})^{-1}\mathbf{B}^T \quad (43)$$

Introducing a compatibility gain parameter g, and premulitplying the strain feedback signal (denoted $^1\mathbf{E}$ in Fig. 2) by $(\mathbf{I} + g\mathbf{I}_{inc})$ strengthens the response of the inner loop control system to the development of strain incompatibilities, without changing the control objective (i.e., out of balance signal entering the controllers will still vanish only when equation (17) (or (39)) is satisfied. It must always be borne in mind, however that such increases in gain have a destabilizing effects on inner control loop dynamics. On the other hand, the intent of the compatibility gain parameter g is not to increase the overall gain on the control system, rather it is to increase the relative emphasis that is placed on enforcement of the compatibility conditions. It is assumed that the overall gains can be adjusted elsewhere in the system (typically in the controllers). In this case, the present control method can be used for all values of Δt ranging from static to dynamic response.

7. CONCLUSIONS

Some possibilities for an on-line analysis test method by which the seismic response of earth structures can be computed without relying on idealized mathematical constitutive laws for the material have been explored. The method is based on a finite element analysis with stress-strain relations that are obtained experimentally as the test proceeds. The influence of the behavior of the soil samples on the dynamic response of the system is taken into account through on-line interaction between the analysis and the tests. Thus the behavior of a soil sample influences the strain history that it experiences in the appropriate way.

Perhaps the currently most promising area of application of this method is in the evaluation of liquefaction potential of horizontally layered soil strata subjected to vertically incident waves. In this case, the stress and strain conditions could be adequately represented with a modest number of soil samples. For more complicated formations, such as an earth dam, some simplification of the problem using Ritz modes becomes a practical necessity.

If dissipation of pore pressure plays an important role, such effects can be accounted for in the analytical part of the procedure, as described in Section 5. In this case the test setups must allow for accurate control of the volumetric strains, which could be achieved by controlling the volume of pore fluid entering or leaving the sample.

The main intent of this paper is to further explore the possibilities of a new approach to evaluating the performance to earth structures, that combines some of the advantages of analysis and testing procedures. In the author's opinion this on-line analysis-test method should complement rather than replace numerical studies and physical modeling techniques.

REFERENCES

1 Akai, K., Ohnishi, Y., Murakami, T. and Horita, M. Coupled stress flow analysis in saturated-unsaturated medium by finite element method, *Number. Methods in Geomech. Aachen, Proc. of the Int Conf., 3rd, Aachen, W. Germany*, Apr. 2-6, Published by A. A. Balkema, Rotterdam, Neth., 1979, **1**, 241-249

2 Boit, M. A. Theory of elasticity and consolidation of a porous anisotropic solid, *Journal of Applied Physics*, 1955, **26**, 182-185

3 Boit, M.A. Theory of propagation of elastic waves in a fluid-saturated porous solid, *The Journal of the Acoustical Society of America*, 1956, **23**, 169-191

4 Boehmer, J. W. and Christian, J. T. Plane Strain Consolidation by Finite Elements, Massachusetts Inst. of Tech., Cambridge, Dept. of Civil Engineering, *Report No. R69-60*, 1969, 183p

5 Elgamal, A. W., Abdel-Ghaffar, A. M. and Prevost, J. H. Elasto-Plastic Earthquake Shear-Response of Earth Dam Models, *Earthquake Engineering & Structural Dynamics*, 1985, **13**(5), 617-633

6 Finn, W. D. L., Lee, K. W. and Martin G. R. An effective stress model for liquefaction, *Liquefaction Problems on Geotechnical Engineering, ASCE National Convention*, Sept. 27-Oct. 1, 1976, 169-198

7 Lacy, S. J. and Prevost, J. H. Nonlinear seismic response analysis of earth dams, *Soil Dynamics and Earthquake Engineering*, 1987, **6**(1), 48-63

8 Liou, C. P., Streeter, V. and Richart, F. A Numerical Model for Liquefaction, *Liquefaction Problems on Geotechnical Engineering*, ASCE National Convention, Sept. 27-Oct. 1, 1976, 313–342

9 Prevost, J. H. Mechanics of continuous porous media, *International Journal of Engineering Science*, 1885, **18**(5), 787–800

10 Prevost, J. H. Effective Stress Analysis of a Seismic Site Response, *International Journal of Numerical and Analytical Methods in Geomechanics*, 1986, **10**(6), 653–665

11 Seed, H. B., Martin P. P. and Lysmer, J. The Generation and Dissipation of Pore Pressures during Soil Liquefaction, *Report no. EERC 75–26*, Earthquake Engineering Research Center, University of California, Berkeley, August, 1975

12 Seed, H. B., Martin, P. P. and Lysmer, J. Pore water pressure changes during soil liquefaction, *Journal of the Geotechnical Engineering Division*, ASCE, 1976, **102**, No GT4, Proc. Paper 12074, April, 323–346

13 Simon, B. R., Wu, J. S. and Zienkiewicz, O. C. Evaluation of higher order, mixed and Hermitean finite element procedures for dynamic analysis of saturated porous media using one-dimensional models, *International Journal for Numerical and Analytical Methods on Geomechanics*, 1986, **10**(5), 483–499

14 Simon, B. R., Zienkiewicz, O. C. and Paul, D. K. Analytical solution for the transient response of saturated porous elastic solids, *International Journal for Numerical and Analytical Methods on Geomechanics*, 1984, **8**(4), 381–398

15 Ueno, M. and Izumi, H Consideration of elasto-plastic constitutive equation for three dimensional deformation analysis of soil and its application, *Proceedings of the Fifth International Conference of Numerical Methods in Geomechanics, Nagoya, Japan*, April 1–5, 1985, published by A. A. Balkema, Rotterdam, Neth., **1**, 325–332

16 Yamazaki, F., Towhata, I. and Ishihara, K. Numerical model for liquefaction problem under Multi-directional shearing in horizontal plane, *Proceedings of the Fifth International Conference on Numerical Methods in Geomechanics, Nagoya, Japan*, 1985 April 1–5, published by A. A. Balkema, Rotterdam, Neth., **1**, 399–406

17 Zienkiewicz, O. C. Numerical Modelling and Geomechanics (Soil–Rock–Concrete), *Mech. of Geomater. Rocks, Concrete, Soils*; Monograph published by John Wiley and Sons, 1985, 471–499

18 Zienkiewicz, O. C. and Shioni, T. Dynamic behavior of saturated porous media: the generalized boit formulation and its numerical solution, *International Journal for Numerical and Analytical Methods in Geomechanics*, 1984, **8**(1), 71–96

19 Hibbitt, Karlsson & Sorensen, Inc., *ABAQUS Manuals: Theory, User's and Examples*, 100 Medway Street, Providence, RI 02906-4402, 1987

20 Duncan, J. M., Seed, R. B., Wong K. S., and Ozawa, Y. FEADAM84: A Computer Program for Finite Element Analysis of Dams, *Geotechnical Engineering Report No. SU/GT/84-03*, Department of Civil Engineering, Stanford University, November, 1984

21 Allard, A., Ph.D. Thesis, California Institute of Technology, in preparation, 1988

22 Katada, T. and Hakuno, M. Nonlinear analysis of surface ground motion by digital control on-line experimental method, *Proc., Eighth World Conference on Earthquake Engineering*, 1984, July 21–28, **III**, 1033–1040

23 Wang, Z., Shen, C. K., Li, X. S. and Yang, H. W. Seismic response analysis of soil deposits by computer on-line testing system – A hybrid system, Proceedings, Third U.S. National Conference on Earthquake Engineering, Charleston, S. C. 1986, August 24–28 **1**, 611–622

24 Thewalt, C. A. and Mahin, S. A. Hybrid Solution Techniques for Generalized Pseudodynamic Testing, University of California, Berkeley, Earthquake Engineering Research Institute, *Report No. UCB/EERC-87/09*, July, 1987,

25 Peek, R. and Yi W. H. Error analysis for the pseudodynamic test method, Part I: Analysis, Part II: Application, *Journal of Engineering Mechanics*, ASCE, **16**(7), July 1990, 1618–1658

26 Newmark, M. N. A method of computation for structural dynamics, *Journal of the Engineering Mechanics Division*, ASCE, 1959, No. EM3, **85**, July

27 Yamada, Y. and Ishihara, K. Anistropic deformation characteristics of sand under three-dimensional stress conditions, *Soils and Foundations*, 1979, **19**(2), 94–97

28 Yamada, Y. and Ishihara, K. Undrained deformation characteristics of loose sand under three-dimensional stress conditions, *Soils and Foundations*, 1981, **21**(1), 97–107

29 Yamada, Y. and Ishihara, K. Yielding of loose sand in three-dimensional stress conditions, *Soils and Foundations*, 1982, **22**(3), 15–31

30 Yamada, Y. and Ishihara, K. Undrained deformation characteristics of sand in multi-directional shear, *Soils and Foundations*, 1983, **23**(1), 61–79

31 Nakai, T., Matsuoka, H., Okuno, N. and Tsuzuki, K. True triaxial tests on normally consolidated clay and analysis of the observed shear behavior using elastoplastic constitutive models, *Soils and Foundations*, 1986, **26**(4), 67–78

32 Shing, P. S. B. and Mahin, S. A. Experimental error propagation in pseudodynamic testing, Earthquake Engineering Research Center, University of California, Berkeley, *Report No. UCB/EERC-83/12*, June 1983

33 Shing, P. S. B. and Mahin S. A. Cumulative experimental errors in pseudodynamic tests, *Earthquake Engineering & Structural Dynamics*, 1987, **15**(4), 409–424

34 Thewalt, C. A. and Mahin, S. A. Hybrid solution techniques for generalized pseudodynamic testing, University of California, Berkeley, Earthquake Engineering Research Institute, *Report No. UCB/EERC-87/09*, July 1987

35 McClamroch, H. N. Displacement control of flexible structures using electro-hydraulic sero-actuators, *Journal of Dynamic Systems, Measurement and Control*, 1985, ASME, **107**, March 34–39

36 McClamroch, H. N. and Hanson, R. D. Control issues for pseudodynamic testing *Presented at the Second International Symposium of Structural Control, Waterloo*, Ontario, Canada, July 16 1985

37 Seed, H. B. Evaluation of soil liquefaction effects on level ground during earthquakes, *Liquefaction Problems in Geotechnical Engineering*, ASCE National Convention, Sept. 27-t. 1, 1976, 1–104

APPENDIX A

The coupled problem of soil deformation and seepage has been studied by a number of investigators[2,3,7,9,18]. Biot[2,3] appears to be the first to have formulated the general three dimensional problem. Since then his formulation has been generalized to include inelastic soil behavior, and finite deformations. Such generalizations follow two different approaches: In the first approach equilibrium equations are derived by considering free bodies whose boundaries do not cut the soil particles. Thus an overall equilibrium equation for the mixture and one for the pore fluid can be derived in terms of the total stresses and pore pressures. The other approach[7,9] is based on mixture theory. In this case the equilibrium equations are typically cast in terms of partial stresses. These partial stresses present the forces transmitted by each medium across a surface that cuts the soil particles. As such these partial stresses are not equal to the total nor the effective stresses.

Zienkiewicz and Shioni[18] also include the effect of compressibility of the soil particles. However their formulation, which is based on a pore pressure coefficient α, is only valid for soils for which there is no coupling between the volumetric or isotropic and the deviatoric parts of the stresses and strains. This assumption is not generally applicable. His formulation could be generalized by introducing a number of coefficients α_{ij} to replace the one α. However, for most problems in soil mechanics, the compressibility of the soil particles is negligible. Indeed compressibility due to imperfect saturation could be much larger than that due to compressibility of the soil grains. Therefore the soil grains are assumed to be incompressible.

For the case that the deformations and pore water motion are small, and the soil particles are incompressible, the author has verified the equations by Zienkiewicz and

Shioni[18], and those by Prevost[9], and also the equivalence of the two approaches. The resulting set of equations can be stated in the following form:

$$-\nabla\cdot\sigma+\rho(b-\ddot{u})-\rho_f\ddot{w}=0 \tag{A1}$$

$$-\nabla p+\rho_f\left(b-\ddot{u}-\frac{1}{n}\ddot{w}\right)-\xi\cdot\dot{w}=0 \tag{A2}$$

$$\nabla\cdot(w+u)+\frac{p}{Q}=0 \tag{A3}$$

in which, b is the body force per unit mass; u is the displacement of the soil skeleton; w is the relative seepage displacement, defined so that the volume of pore fluid per unit area the passes through a surface that moves with the soil skeleton is equal to the projection of w in the direction normal to that surface; σ is the soil mechanicians' total stress tensor, defined so that the traction on a surface with unit outward normal ν is $t=-\sigma\cdot\nu$; p is the pore pressure; n is the porosity; ρ and ρ_f are the mass densities for the mixture and the pore fluid respectively; ξ is Stoke's drag tensor, which is related to Darcy's permeability tensor k through $\xi=\rho_f g k^{-1}$; finally, $Q=k_s/n$ where k_s is the bulk modulus of the pore fluid.

Using the effective stress principle, $\sigma=\sigma'+p\delta$, where σ' is the soil mechanician's effective stress tensor and δ is the identity tensor, equations (A1) to (A3) can be reduced to

$$-\nabla\cdot\sigma'+\nabla(Q\nabla\cdot(w+u))+\rho(b-\ddot{u})-\rho_f\ddot{w}=0 \tag{A4}$$

$$\nabla(Q\nabla\cdot(w+u))+\rho_f\left(b-\ddot{u}-\frac{1}{n}\ddot{w}\right)-\xi\cdot\dot{w}=0 \tag{A5}$$

As is usual in finite elements formulations, the displacement fields are written in terms of nodal values as follows:

$$u_i=N^A u_i^A \tag{A6}$$

$$w_i=N^A w_i^A \tag{A7}$$

in which u_i and w_i are the components of u and w in the ith coordinate direction (cartesian coordinates); N^A is the interpolation function for node A; and u_i^A and w_i^A are the ith component of the nodal values of u and w respectively, at node A. Summation over all nodes on the mesh for the repeated index A is implied.

Standard procedures of finite element discretization lead to:

$$\begin{pmatrix}\mathbf{s}\\ \cdot\end{pmatrix}+\begin{pmatrix}\mathbf{K}_f & \mathbf{K}_f\\ \mathbf{K}_f & \mathbf{K}_f\end{pmatrix}\begin{pmatrix}\mathbf{d}_s\\ \mathbf{d}_f\end{pmatrix}+\begin{pmatrix}\cdot & \cdot\\ \cdot & \mathbf{C}\end{pmatrix}\begin{pmatrix}\mathbf{v}_s\\ \mathbf{v}_f\end{pmatrix}+\begin{pmatrix}\mathbf{M} & \mathbf{M}_f\\ \mathbf{M}_f & \mathbf{M}_{ff}\end{pmatrix}\begin{pmatrix}\mathbf{a}_s\\ \mathbf{a}_f\end{pmatrix}=\begin{pmatrix}\mathbf{f}\\ \mathbf{f}_f\end{pmatrix} \tag{A8}$$

in which $\mathbf{d}_s$, $\mathbf{v}_s$, $\mathbf{a}_s$ and $\mathbf{d}_f$, $\mathbf{v}_f$, $\mathbf{a}_f$ are the nodal displacements, velocities and accelerations for the soil skeleton (subscript s) and the pore fluid (subscript f) respectively, and the elements of the various submatrices in equation (A8) are given by

$$\mathrm{f}_i^A=\int_\Omega N^A\rho b_i dV+\int_\Gamma t_i N^A\,dS \tag{A9}$$

$$f_{fi}^A=\int_\Omega N^A\rho_f b_i dV-\int_\Gamma v_i p N^A dS$$

$$s_i'^A=-\int_\Omega \sigma'_{ik}N^A_{,k}dV \tag{A11}$$

$$C_{ij}^{AB}=\int_\Omega N^A\xi_{ij}N^B dV \tag{A12}$$

$$K_{fij}^{AB}=\int_\Omega N^A_{,i}QN^B_{,j}dV \tag{A13}$$

$$M_{ij}^{AB}=\int_\Omega N^A\rho\delta_{ij}N^B dV \tag{A14}$$

$$M_{fij}^{AB}=\int_\Omega N^A\rho_f\delta_{ij}N^B dV \tag{A15}$$

$$M_{nij}^{AB}=\int_\Omega N^A\frac{1}{n}\rho_f\delta_{ij}N^B dV \tag{A16}$$

in which $(.)_{,k}$ denotes the partial derivative of (.) in the kth coordinate direction; t_i is the ith component of the total traction vector t (includes forces on pore fluid as well as soil skeleton); Ω is the region of saturated soil under consideration; Γ is the entire boundary of Ω; and δ_{ij} is the Kronecker Delta. It is further understood that for any matrix (.), $(.)_{ij}^{AB}$ denotes the element of that matrix in the row corresponding the ith coordinate direction at node A, and the column corresponding to the jth coordinate direction at node B.